*Sensors and Materials*, Vol. 19, No. 2 (2007) 107–121
MYU Tokyo

S & M 0669

# Transverse Electromagnetic Microactuators Using Electroplated Planar Coil Driven by Symmetric Twin Magnets

Ji-Chul Ryu and Young-Ho Cho*

Digital Nanolocomotion Center, Department of BioSystems
Korea Advanced Institute of Science and Technology
373-1 Guseong-dong, Yuseong-gu, Daejeon 305-701, Republic of Korea

(Received September 20, 2006; accepted February 21, 2007)

***Key words:*** electromagnetic microactuator, radial magnetic field, twin magnets, electroplating

In this paper, we present an electromagnetic microactuator that uses an electroplated copper coil on a $p^+$-silicon diaphragm with symmetric twin magnets. The microactuator generates a vertical motion of the diaphragm using the radial components of the magnetic field on the coil plane. To guide and concentrate the magnetic field in the radial direction, we propose a new microactuator structure with symmetric twin magnets. The microactuator shows values of resonant frequency and quality factor in the ranges of 10.51±0.22 kHz and 46.6±3.3, respectively. The twin magnet microactuator generates the maximum peak-to-peak amplitude of 4.4 μm for an AC rms current of 26.8 mA, showing 2.4 times larger amplitude than the single magnet microactuator.

## 1. Introduction

Recently, a wide variety of microfluidic devices,[1–16] such as micropumps and microvalves, have been developed for applications in precision biofluid control and microflow regulation. In microfluidic devices, various actuation principles are employed to transport microfluid, and include thermopneumatic,[2–4] electrostatic,[5–7] piezoelectric,[8–10] bimetallic,[11–12] and electromagnetic[13–16] methods.

In this work, we consider the electromagnetic method, suitable to transport biofluid for biomedical applications. Thermopneumatic or bimetallic actuators may generate high temperatures (over 100°C[4]), causing fatal damage to the bioobjects being transported. Electrostatic actuators may result in unwanted modification of the bioobjects owing to the large electric field. Piezoelectric actuators also have limited applications because it is require very high voltage.

*Corresponding author: e-mail: nanosys@kaist.ac.kr

Recently, there have been research activities on electromagnetic actuators. Wagner *et al.*[13] presented an electromagnetic microactuator that uses a magnet (NdFeB) bonded to a suspended silicon diaphragm surrounded by a fixed external planar coil. The vertical motion of the magnet is obtained using the magnetic field produced by an external coil. Using a similar actuation principle, Yanagisawa *et al.*[14] developed an electromagnetically driven microvalve. Meckes *et al.*[16] presented another type of electromagnetic actuator for use in microvalves, where a planar coil on the diaphragm is placed over a fixed single permanent magnet.

Conventional electromagnetic microactuators[15–16] have used a single magnet (Fig. 1(a)) to provide a radial magnetic field in the coil plane for the electromagnetic actuation in the direction normal to the magnet. In the present study, however, we use twin magnets (Fig. 1(b)) to guide and concentrate the magnetic field in the radial direction required for producing a large vertical motion of the planar coil. Compared with the conventional microactuators using a single magnet (Fig. 1(a)), the present microactuator using twin magnets (Fig. 1(b)) generates a large force for a given electric current owing to the condensed magnetic field in the radial direction in the coil plane. The twin-magnet microactuator also shows the potential for low power consumption owing to the lower electric current required for producing an identical electromagnetic force.

## 2. Theoretical Analysis

### 2.1 *Electromagnetic Force*

Figure 2 illustrates the structure of the electromagnetic microactuator proposed in this paper. The planar spiral coil on the diaphragm has been placed in the magnetic field formed by two permanent magnets. A coil current generates an electromagnetic force, deflecting the silicon diaphragm in the direction normal to the substrate using the magnetic field component in the radial direction.

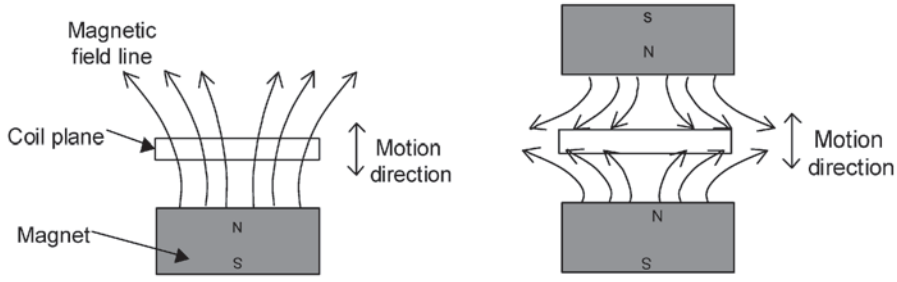


Fig. 1. Electromagnetic microactuators driven by radial magnetic field: (a) Conventional structure with single magnet; (b) Proposed structure with twin magnets.

The electromagnetic force, $\vec{F}$, generated by the spiral coil in the magnetic field, $\vec{B}$, can be obtained from the integration of the force generated on a coil segment, $\vec{dl}$, along the spiral coil:

$$\vec{F} = \int d\vec{F} = \int id\vec{l} \times \vec{B}, \tag{1}$$

where $i$ is the coil current.

In Fig. 2, the force in the direction normal to the magnets produces a diaphragm deflection in convex and concave shapes. Since the magnetic field in the radial direction is perpendicular to the spiral coil, the coil current generates the diaphragm motion in the $z$-direction. For an axisymmetric magnetic field distribution on the coil plane, the magnitude of the magnetic force is a function of the radial distance from the coil center. For mathematical simplicity, the spiral coil is considered as a set of concentric circles of identical turns. The total vertical force on the concentric coils is expressed as

$$F_{total} = \sum_{k=1}^{n} F_k = \sum_{k=1}^{n} i(2\pi r_k) B_k \tag{2}$$

where $n$ is the number of coil turns, $F_k$ is the electromagnetic force on the $k$ th turn of the coil, $r_k$ is the radius of the $k$ th turn of the coil, and $B_k$ is the magnitude of the magnetic field in the radial direction along the circle of radius $r_k$.

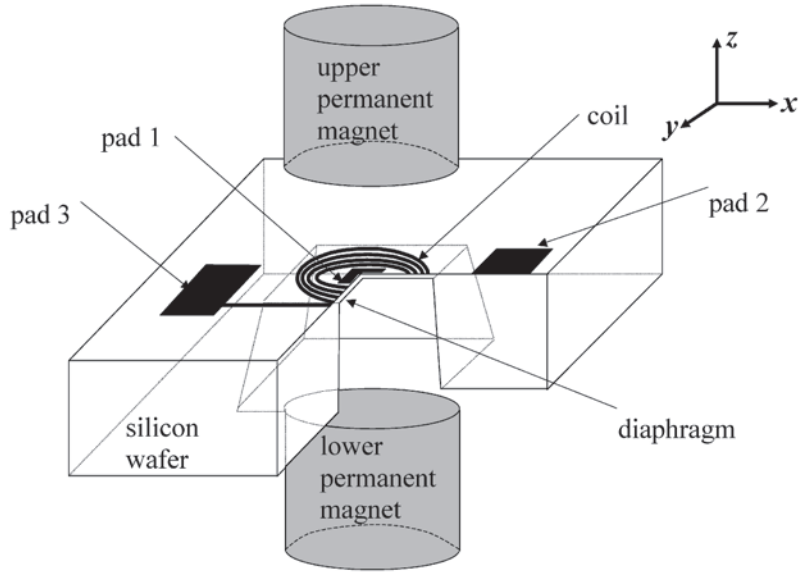


Fig. 2. Perspective view of proposed electromagnetic microactuator where radial magnetic field is guided and concentrated by twin magnets.

The total length of the simplified coil model, $l_s$, is compared with that of the actual coil, $l_a$, as follows.

$$l_s = \sum_{k=1}^{n} 2\pi r_k = \frac{\pi}{p}\left[r_o^2 - r_i^2 + p(r_o + r_i)\right] \tag{3a}$$

$$l_a = \int r d\theta = \int_{\theta_i}^{\theta_o} \left(\frac{p}{2\pi}\theta\right) d\theta = \frac{\pi}{p}(r_o^2 - r_i^2) \tag{3b}$$

where $p$, $n$, $r_i$, $r_o$, and $\theta$ denote the pitch of the coil, the number of coil turns, the inner radius of the coil, the outer radius of the coil and the angle of the coil, respectively. From a comparison of eqs. (3a) and (3b) using eq. (1), we find that the net magnetic force for the simplified coil model of eq. (3a) overestimates the value for the spiral coil model of eq. (3b). With the assumption of a uniformly distributed magnetic field with respect to the radial direction, the error between the electromagnetic force of the simplified coil model and that of the actual spiral coil is defined by

$$error = \frac{l_c - l_a}{l_a} \times 100\% = -\,p\,\frac{1}{r_o - r_i} \times 100\% \tag{4}$$

## 2.2 *Static Response*

For a uniformly loaded square diaphragm on the $x$-$y$ plane, the deflected shape[17] is assumed to be as follows.

$$u = C \sin\frac{\pi x}{a} \cos\frac{\pi y}{2a} \tag{5a}$$

$$v = C \sin\frac{\pi y}{a} \cos\frac{\pi x}{2a} \tag{5b}$$

$$w = w_o \cos\frac{\pi x}{2a} \cos\frac{\pi y}{2a} \tag{5c}$$

where $C$ is a constant; $u$, $v$ and $w$ are the deflections in $x$-, $y$- and $z$-directions at the point ($x$, $y$) on the diaphragm; $a$ is the half-edge length; $w_o$ is the maximum deflection in the $z$-direction of the square diaphragm.

For the assumed diaphragm deflections of eq. (5), the virtual work theory based on the strain energy in the diaphragm results in the load-deflection relationship. From a comparison of the experimental deflection and finite-element method (FEM) results,[18] we corrected the coefficients of the load-deflection relationship as follows.

$$P = 3.41\,\frac{t\sigma_o w_o}{a^2} + 1.37(1.446 - 0.427\nu)\,\frac{E}{1-\nu}\,\frac{tw^3}{a^4} \tag{6}$$

where $P$ is the uniformly applied pressure; $t$ is the thickness of diaphragm; $\sigma_o$ is the residual stress; $w_o$ is the center deflection; $a$ is the half-edge length of the diaphragm;

$E$ is the Young's modulus; $v$ is the Poisson's ratio. In eq. (6), we assume that the coil on the diaphragm does not affect the deflected shape of the diaphragm. The total electromagnetic force of eq. (2) divided by the total area of the diaphragm is considered as the uniform pressure, $P$, of eq. (6).

### 2.3 *Dynamic Response*

The natural frequency of the coil diaphragm can be estimated as follows. First, for a diaphragm with clamped edges, the natural frequency is obtained from the conventional diaphragm theory[19] as

$$f_o = \frac{\lambda}{2\pi (2a^2)} \left[ \frac{Et^3}{12\gamma (1 - v^2)} \right]^{1/2} \tag{7a}$$

where $\lambda$ is the normalized natural frequency, defined as 35.99 for a clamped rectangular diaphragm and $\gamma$ is the mass per unit area of the diaphragm. Equation (7a) is valid for a clamped diaphragm without an in-plane load or residual stress. With the consideration of an in-plane load or residual stress, the natural frequency of the diaphragm is modified[19] to be

$$f = \left[ f_o^2 + \frac{NJ}{2\gamma (2a)^2} \right]^{1/2} \tag{7b}$$

where $f_o$ is the natural frequency without an in-plane load or residual stress, $N$ is the in-plane load per unit edge length of the diaphragm, and $J$ is a dimensionless coefficient depending on the mode number and the boundary conditions, whose value is defined as 1.248[19] for a clamped rectangular diaphragm in the first mode of deflection.

From Rayleigh's method, the natural frequency of a diaphragm can be obtained from the consideration of kinetic and potential energies. The kinetic energy is associated with the mass of the diaphragm and the potential energy is related to the strain energy. From the strain energy, based on static deflection due to gravity,[19] the natural frequency is expressed in terms of the deflection of the structure under its own weight:

$$f = \frac{1}{2\pi} \sqrt{\frac{g}{\delta_s}} \tag{7c}$$

where $g$ and $\delta_s$ are the acceleration due to gravity and the static deflection of the diaphragm due to gravity, respectively. Jones[20] and Johns[21] suggest that the fundamental frequency of a thin uniform diaphragm can be corrected as follow

$$f = \frac{1.277}{2\pi} \sqrt{\frac{g}{\delta_s}} \tag{7d}$$

For small damping ($\xi$<0.05), the static deflection, $\delta_{st}$, and the dynamic amplitude at resonance, $X$, is related to the quality factor ($Q$-factor) of the system as follows

$$\left(\frac{X}{\delta_{st}}\right) = Q \tag{8}$$

Using eq. (8) with the measured $Q$-factor, we can obtain the theoretical dynamic amplitude at the resonant frequency from the estimated static deflection of eq. (6).

## 3. Microactuator Disign

From the consideration of the mechanical strength and fabrication process of the diaphragm, the thickness of the boron-diffused diaphragm was chosen to be 5 μm. From previous study of silicon diaphragm micropumps,[6–10] we found that the ratio of the single-stroke volume to the total chamber volume is in the range of $0.625\times10^{-3}$ to $6.25\times10^{-3}$. Since the single-stroke fluid volume and the total chamber volume are related to the size of the silicon diaphragm, we chose the half-edge length, $a$, of the diaphragm to be 2 mm.

For the 4 mm × 4 mm diaphragm, a magnet 5 mm in diameter and 5 mm in height was chosen. To measure the deflection of the diaphragm, a hole with a radius of 1 mm was drilled through the upper magnet. The inner radius of the coil was chosen as 1 mm, which is identical to the radius of the hole in the upper magnet. The outer coil radius was chosen as 1.5 mm so that the deflection contour near the diaphragm center would be circular in shape. To increase the net coil length, the coil width and inter-coil gap were chosen to be the same as the minimum line width of 25 μm, allowing for the emulsion mask pattern. To increase the cross-sectional area of the coil for a higher-electric-current drive, we chose the coil height as 30 μm, which is the maximum for the reproducible electroplating process.

We fixed the gap between a magnet and diaphragm to 1 mm, which is a conventional biochip thickness composed several layers. The electromagnetic force depends on the gap. But it is fixed in our case, where the magnets are attached to the chip.

## 4. Fabrication Process

The present electromagnetic microactuator (Fig. 2) consists of an electroplated copper coil on a $p^+$-silicon diaphragm and two permanent magnets. The permanent magnets are Nd-Fe-B-type magnets, and the maximum magnitude of the magnetic field is 0.5 T. Figure 3 illustrates the microfabrication process for the coil and the $p^+$-silicon diaphragm.

The fabrication starts with 520-μm-thick, 4″ (100) silicon wafers. In Fig. 3(a), the 5-μm-thick $p^+$-silicon diaphragm is defined by the boron diffusion process performed at 1100°C for 9 h. A 2500-Å-thick LPCVD $Si_3N_4$ layer is deposited as the electrical isolation layer as well as the mask layer of the EDP back-side etching process for diaphragm definition. In Fig. 3(b), the etch window for the 4 mm × 4 mm square diaphragm is patterned by the RIE process. In Fig. 3(c), 200-Å/1200-Å-thick Cr/Cu layer is evaporated as the seed layer of the electroplating process for the copper coil. In Fig.

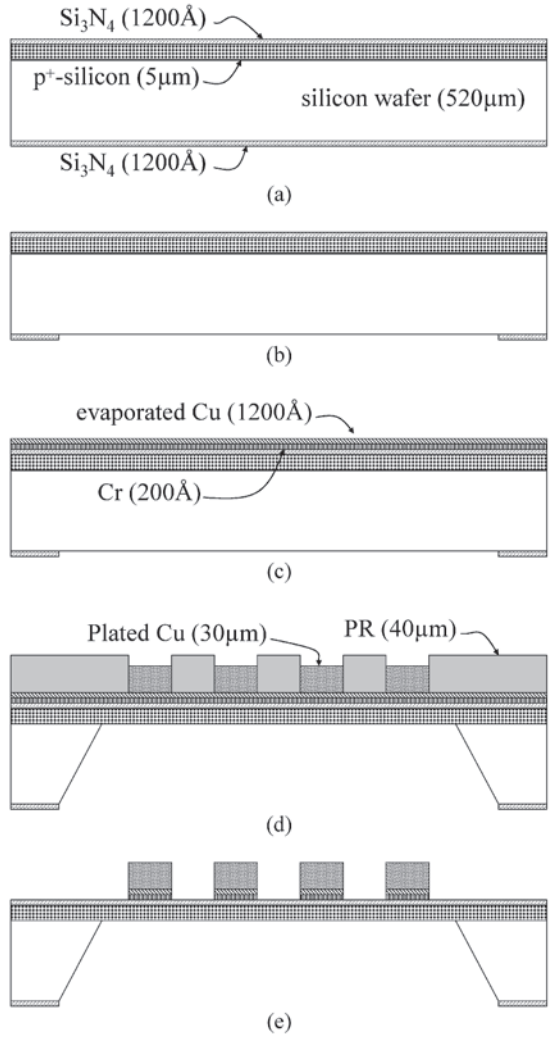


Fig. 3. Fabrication process for electroplated planar coil on diaphragm: (a) boron doping and Si3N4 deposition; (b) RIE of Si3N4 for etch window opening; (c) Cr/Cu seed layer evaporation; (d) thick PR patterning and Cu plating; (e) Cr/Cu seed layer etching and back-side silicon etching.

3(d), thick PR is coated and patterned to obtain the mold for the electroplated coil. After the removal of the Cr/Cu layer, back-side etching of the silicon substrate is processed in EDP solution to fabricate the coil diaphragm of the microactuator, as shown in Fig. 3(e). Figure 4 shows a top view of the fabricated microcoil on the square diaphragm of the microactuator. The electrical resistance of the fabricated microcoil is measured in the

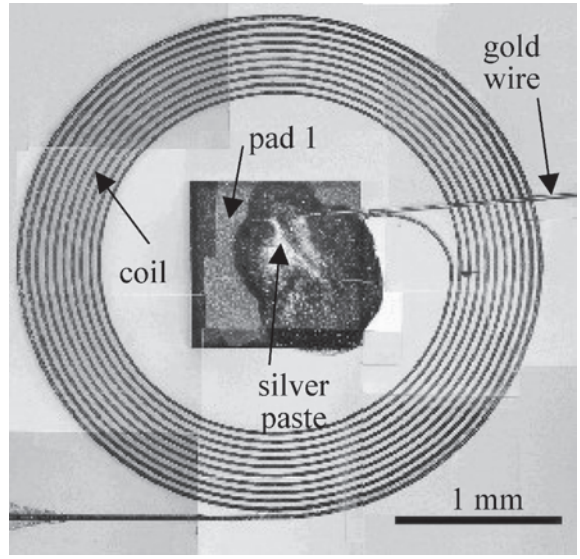


Fig. 4. Top view of fabricated microactuator, where gold wire provides electrical interconnection.

range of 0.2–0.4 Ω and applied current is 26.8 mA. Thus, total heat generation rate is in the range of 0.14–0.29 mW, which is too low to generate temperature change in water solution.

## 5. Theoretical Response Estimation

Using the dimensions measured from the fabricated structure, we estimate the natural frequency, the electromagnetic force and the static deflection of the microactuator. Table 1 lists the natural frequencies, estimated from eqs. (7a), (7b), and (7d), respectively. The first estimation is based on a model without in-plane loads (*e.g.*, residual stresses of thin films) and the other estimations are based on a model considering in-plane loads. As shown in Table 1, there are large discrepancies between the estimated natural frequencies considering the effect of residual stresses and those without considering them. Thus, we should consider the effect of residual stresses when we estimate the natural frequency of the micromachined diaphragm actuators.

Using an electromagnetics analysis program (Maxwell 3D 4.0), we analyzed the magnetic field in the radial direction, obtaining the upward and downward forces for the permanent magnet compositions in Fig. 5. The results obtained for the three cases in Fig. 5, including the single magnet without a hole (S0), twin magnets without a hole (T0) and twin magnets with a hole (T1), are compared in Fig. 6. The strength of the permanent magnet is 0.5 T.

Table 1.
Estimated natural frequencies of coil diaphragm.

| Loading conditions | Natural frequency |
|---|---|
| Without in-plane loads | 0.927 kHz |
| With in-plane loads | 13.9 kHz |
| With static deflections | 13.1 kHz |

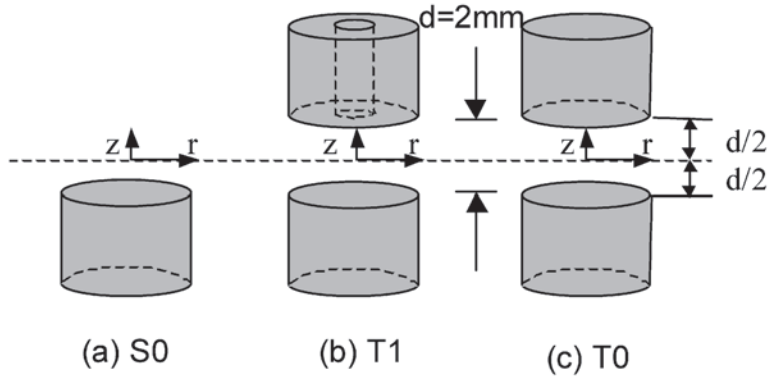


Fig. 5. Magnet compositions for radial magnetic field on coil plane at $z$=0: (a) single magnet; (b) twin magnets with single hole; (c) twin magnets without hole.

From Fig. 6, we find that the case of twin magnets without a hole (T0) provides the largest radial magnetic field of the three cases. The radial magnetic field for the case of T0 is 100% greater than the value for the single magnet. Based on eq. (2) and the linear fitting of radical-dependent magnetic field of Fig. 6, the net electromagnetic force generated by the coil is calculated as 9.554$i$ mN for the single magnet case (S0), 14.158$i$ mN for the twin magnets with a single hole (T1), and 19.145$i$ mN for the twin magnets without a hole (T0), where $i$ is the coil current. The electromagnetic force current obtained for varying coil current is shown in Fig. 7. The error between the electromagnetic force of the simplified coil model (eq. (2)) and the actual electromagnetic force is estimated as 5% from eq. (4).

## 6. Experimental Results and Discussion

Figure 8 shows the experimental setup for the peak-to-peak amplitude measurement of the microactuators, where the detection sensitivity is 20 μm/V with a detection resolution of 0.08 μm for the peak-to-peak full-scale output of 320 μm. To hold the

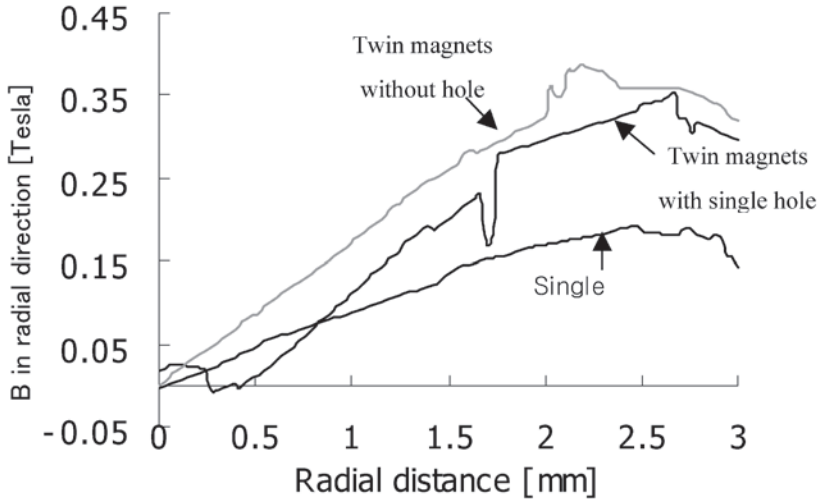


Fig. 6. Magnitude of radial magnetic field along radial direction in plane.

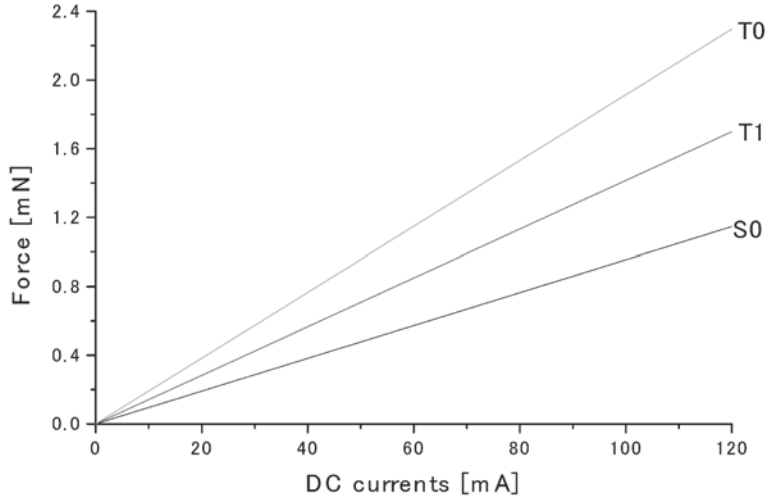


Fig. 7. Estimated electromagnetic force for varying DC coil current.

magnets in an exact position, we used a jig for the positioning of the two permanent magnets and fabricated device.

Figure 9 shows the measured frequency response function of the electromagnetic actuator with a single hole (S0). For the case of the single magnet (S0), the resonant frequency and *Q*-factor were measured as 10.51±0.06 kHz and 45.9±2.1, respectively. For the case of the twin magnets with a single hole (T1), the resonant frequency and *Q*-factor were obtained as 10.51±0.22 kHz and 46.6±3.3, respectively. The measured

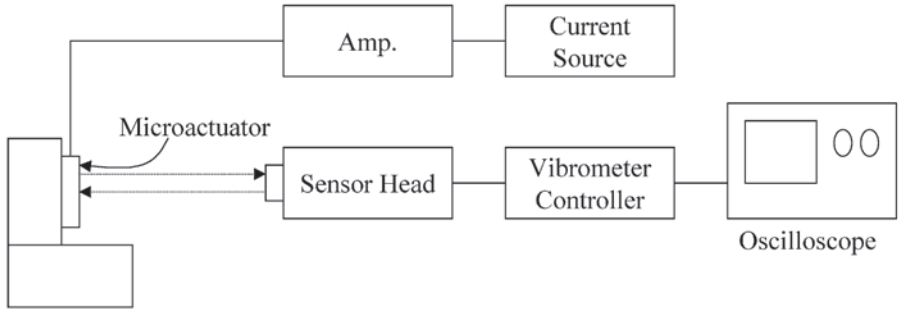


Fig. 8. Instrumental setup for measurement of dynamic response of microactuator.

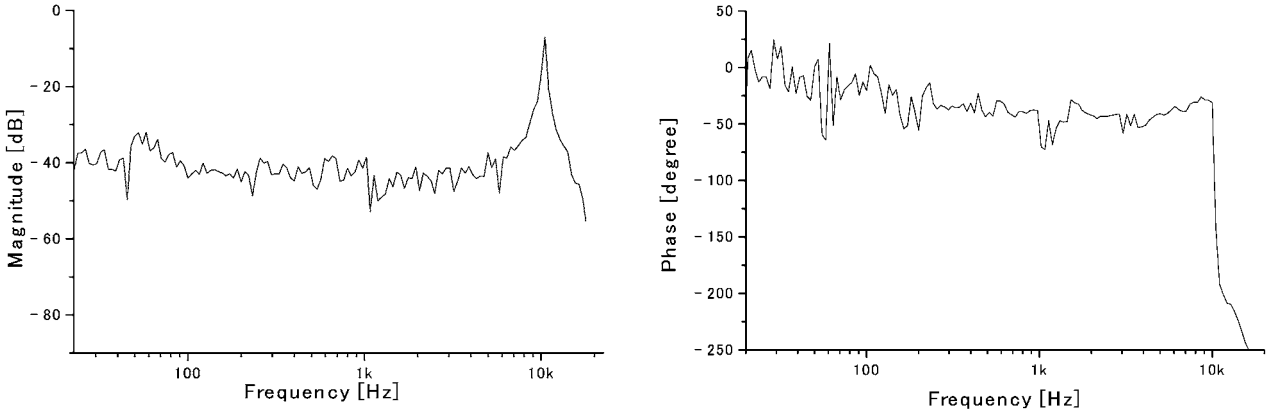


Fig. 9. Frequency response function of electromagnetic actuator: (a) amplitude response; (b) phase response.

performance characteristics of the microactuators are summarized in Table 2.

The peak-to-peak amplitude of the microactuators has been measured for varying coil current. Figures 10 and 11 show the results measured at 10.6 kHz. From a comparison of S0 (Fig. 10) and T1 (Fig. 11), we observed that the peak-to-peak amplitude for the single magnet is larger than that for the twin magnets with a single hole. From the simulation of the magnetic field distribution for the case of twin magnets with a single hole (T1 in Fig. 5(b)), we found that the magnitude of the magnetic field decreases markedly toward the magnet with a hole (Fig. 12). Since the magnitude of the magnetic field in the radial direction is constant from $z = 0$ to $z = -1$ mm (Fig. 12), we repeat the experiment after moving the lower magnet toward the coil plane by 450 μm. In the new experiment, we found that the peak-to-peak amplitudes measured for T1 are larger than those for S0 (Fig. 13). The measured peak-to-peak amplitude for the case of the twin

Table 2
Electromagnetic actuation characteristics of fabricated microactuator.

| Magnet composition | Resonant frequency [kHz] | Quality factor | Peak-to-peak amplitude at resonance [μm] |
|---|---|---|---|
| S0 | 10.51±0.06 | 45.9±2.1 | 1.8* |
| T1 | 10.51±0.22 | 46.6±3.3 | 4.4** |

*measured at rms AC drive current of 25.5 mA
**measured at rms AC drive current of 26.8 mA

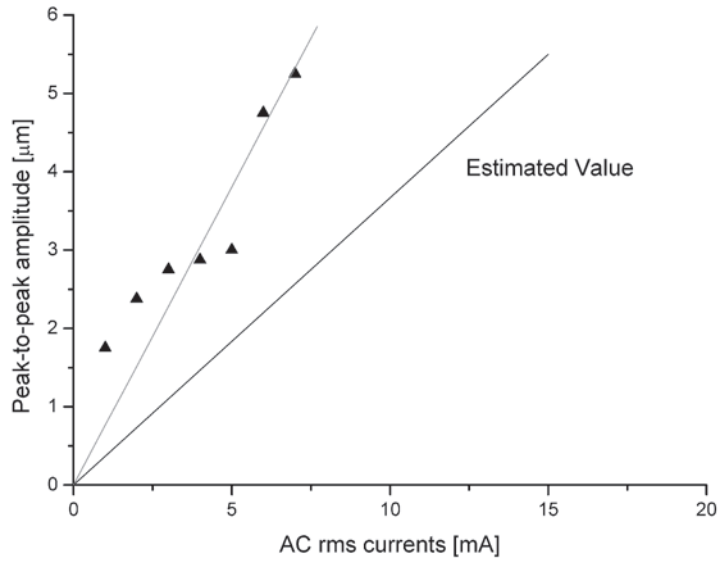


Fig. 10. Measured and estimated peak-to-peak amplitude of microactuator for varying AC coil current at resonant frequency of 10.6 kHz for case of single magnet (S0).

magnets (T1 in Fig. 5(b)) is about 2.4 times larger than that for the single magnet at an rms AC current of 26.8 mA.

However, in Figs. 10, 11, and 13, there are some discrepancies between estimated values and measured values. The first reason is that we assumed the electromagnetic force to be a uniformly distributed load to estimate the theoretical values, but, in the experimental study, the electromagnetic force is applied only at the position of the coil. The second reason is that, when we estimated the deformation and displacement of the diaphragm, we assumed the rectangular diaphragm model, which has a uniform thickness and isotropic material properties. In fact, the fabricated diaphragm of microactuator does

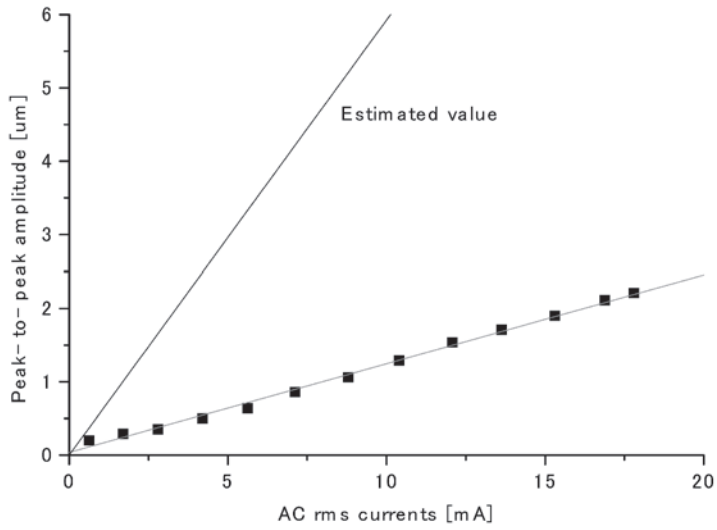


Fig. 11. Measured and estimated peak-to-peak amplitude of microactuator for varying AC coil currents at resonant frequency of 10.6 kHz for case of twin magnets with single hole (T1).

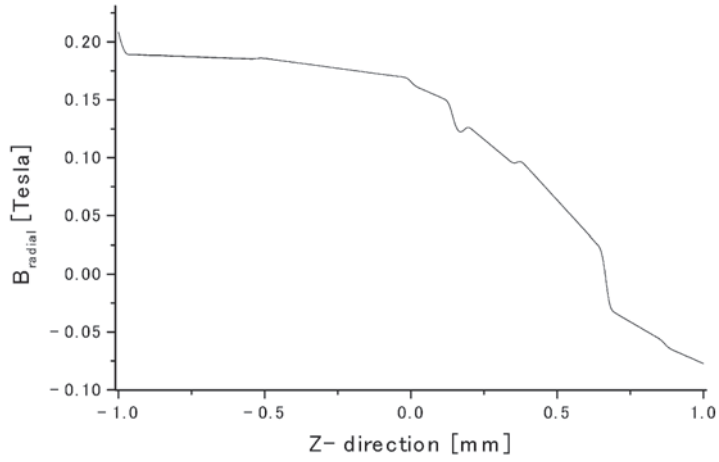


Fig. 12. Estimated magnitude of radial field along z-direction for case of twin magnets with single hole.

not have a uniform thickness and isotropic material properties, owing to the electroplated copper spiral coil on the silicon diaphragm. Finally, we transfigured the spiral shape of the coil to the set of concentric circles of identical turns, as mentioned in eq. (4). The discrepancy from the transfiguring of the coil shape can be estimated as 5% from eq. (4).

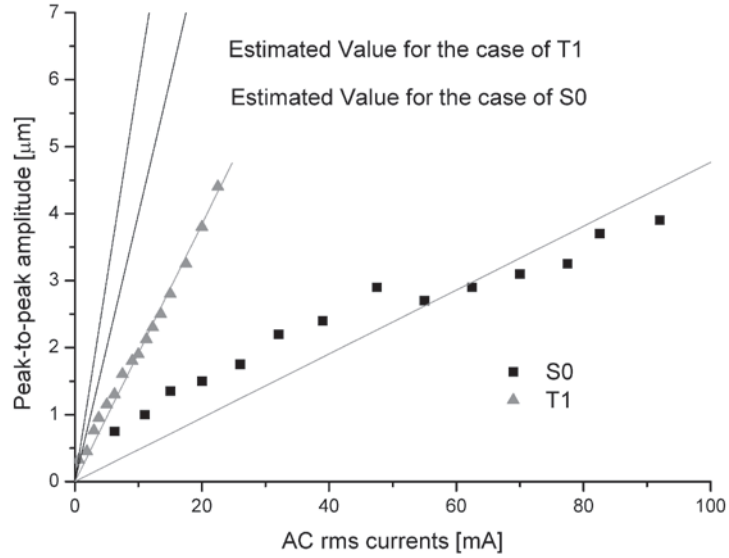


Fig. 13. Measured and estimated peak-to-peak amplitude of microactuator for varying AC coil currents at resonant frequency of 10.51 kHz. The lower magnets are raised by 450 μm from the position in the cases of S0 and T1 in Fig. 5.

## 7. Conclusions

In this paper, we presented, fabricated, and tested an electromagnetic microactuator that uses an electroplated copper coil diaphragm driven by symmetric twin magnets. The microactuator utilized the radial magnetic field formed between two permanent magnets. In the theoretical analysis, we derived the electromagnetic force of the microactuator and the static response as well as the dynamic response of the microactuator. In the experimental analysis, we measured and compared the dynamic response of the microactuator with estimated values. The amplitude and phase response of the microactuators were measured for the cases of twin magnets and a single magnet, respectively. For the case of the single magnet, the resonant frequency and *Q*-factor were obtained as 10.51±0.06 kHz and 45.9±2.1, respectively. For the case of the twin magnets with a single hole, the resonant frequency and *Q*-factor were measured as 10.51±0.22 kHz and 46.6±3.3, respectively. The presented twin-magnet structure was effective in concentrating and guiding the magnetic field in the radial direction. The peak-to-peak amplitude for the twin magnets with a single hole was measured as 2.4 times that for the single magnet for an identical AC rms current drive of 26.8 mA. In addition, the precise control of microflow is possible for the microactuator by changing the magnitude of the input current at a fixed current frequency.

## References


1 S. Shoji: Topics in Current Chemistry **194** (1998) 163.
2 T. S. J. Lammerink, M. Elwenspoek and J. H. J. Fluitman: Proc. IEEE MEMS Workshop (Fort Lauderdale, 1993) p. 245.
3 T. G. Kang, K.-S. Seo, Y.-H. Cho, O H. Baek, W. L. Hwang and J. H. Moon: Proc. Actuator ' 98 (Bremen, 1998) p. 62.
4 W. K. Schomburg, R. Ahrens, W. Bacher, S. Engemann, P. Krehl and J. Martin: Proc. Transducers '97 (Chicago, 1997) p. 365.
5 M. A. Huff, M. S. Mettner, T. A. Lober and M. A. Schemidt: Proc. Solid-State Sensor and Actuator Workshop (Hilton Head Island, 1990) p. 123.
6 R. Zengerle, A. Richter and H. Sandmaier: Proc. IEEE MEMS Workshop (Travemunde, 1992) p. 19.
7 R. Zengerle, S. Kluge, M. Richter and S. Richter: Proc. IEEE MEMS Workshop (Amsterdam, 2995) p. 19.
8 J. G. Smits: Sensors and Actuators A **21** (1990) 203.
9 M. Koch, N. Harris, A. G. R. Evans, N. M. White and A. Brunnschweiler: Proc. Transducers '97 (Chicago, 1997) p. 353.
10 R. Linnemann, P. Woias, C.-D. Senfft and J. A. Ditterich: Proc. IEEE MEMS Workshop (Heidelberg, 1998) p. 532.
11 W. Benecke and W. Riethmuller: Proc. IEEE MEMS Workshop (Salt Lake city, 1989) p. 116.
12 H. Jerman: Proc. Solid-State Sensor and Actuator Workshop (Hilton Head Island, 1990) p. 65.
13 B. Wagner and W. Benecke: Proc. IEEE MEMS Workshop (Nara, 1991) p. 27.
14 K. Yanagisawa, H. Kuwano and A. Tago: Proc. Transducers '93 (Yokohama, 1993) p. 102.
15 J. Behrens, A. Meckes and W. Benecke: Micro System Technologies 96 (Potsdam, 1996) p. 820.
16 A. Meckes, J. Behrens and W. Benecke: Actuators 98 (Bremen, 1998) p. 152.
17 S. Timoshenko and S. Woinowsky-Krieger: Theory of Plate and Shells (McGraw-Hill International Book Company, Tokyo, 1970) 2nd ed., p. 420.
18 J. Y. Pan, P. Lin, F. Maseeh and S. D. Senturia: Proc. IEEE Solid-State Sensor and Actuator Workshop (Hilton Head Island, 1990) p. 70.
19 R. D. Blevins: Formulas for Natural Frequency and Mode Shape (Van Nostrand Reinhold Company, NY, 1979) 1st ed., p. 261.
20 R. Jones: Journal of Sound and Vibration **38** (1975) 503.
21 D. J. Johns: Journal of Sound and Vibration **41** (1975) 385.